HO_x chemistry during INTEX-A 2004: Observation, model calculation, and comparison with previous studies

Xinrong Ren,[1,2] Jennifer R. Olson,[3] James H. Crawford,[3] William H. Brune,[1] Jingqiu Mao,[1] Robert B. Long,[1] Zhong Chen,[1] Gao Chen,[3] Melody A. Avery,[3] Glen W. Sachse,[3] John D. Barrick,[3] Glenn S. Diskin,[3] L. Greg Huey,[4] Alan Fried,[5] Ronald C. Cohen,[6] Brian Heikes,[7] Paul O. Wennberg,[8] Hanwant B. Singh,[9] Donald R. Blake,[10] and Richard E. Shetter[11]

Received 13 July 2007; revised 24 October 2007; accepted 18 December 2007; published 8 March 2008.

[1] OH and HO_2 were measured with the Airborne Tropospheric Hydrogen Oxides Sensor (ATHOS) as part of a large measurement suite from the NASA DC-8 aircraft during the Intercontinental Chemical Transport Experiment-A (INTEX-A). This mission, which was conducted mainly over North America and the western Atlantic Ocean in summer 2004, was an excellent test of atmospheric oxidation chemistry. The HOx results from INTEX-A are compared to those from previous campaigns and to results for other related measurements from INTEX-A. Throughout the troposphere, observed OH was generally 0.95 of modeled OH; below 8 km, observed HO_2 was generally 1.20 of modeled HO_2. This observed-to-modeled comparison is similar to that for TRACE-P, another midlatitude study for which the median observed-to-modeled ratio was 1.08 for OH and 1.34 for HO_2, and to that for PEM-TB, a tropical study for which the median observed-to-modeled ratio was 1.17 for OH and 0.97 for HO_2. HO_2 behavior above 8 km was markedly different. The observed-to-modeled HO_2 ratio increased from $\sim$1.2 at 8 km to $\sim$3 at 11 km with the observed-to-modeled ratio correlating with NO. Above 8 km, the observed-to-modeled HO_2 and observed NO were both considerably greater than observations from previous campaigns. In addition, the observed-to-modeled HO_2/OH, which is sensitive to cycling reactions between OH and HO_2, increased from $\sim$1.5 at 8 km to almost 3.5 at 11 km. These discrepancies suggest a large unknown HO_x source and additional reactants that cycle HO_x from OH to HO_2. In the continental planetary boundary layer, the observed-to-modeled OH ratio increased from 1 when isoprene was less than 0.1 ppbv to over 4 when isoprene was greater than 2 ppbv, suggesting that forests throughout the United States are emitting unknown HO_x sources. Progress in resolving these discrepancies requires a focused research activity devoted to further examination of possible unknown OH sinks and HO_x sources.

Citation: Ren, X., et al. (2008), HO_x chemistry during INTEX-A 2004: Observation, model calculation, and comparison with previous studies, *J. Geophys. Res.*, *113*, D05310, doi:10.1029/2007JD009166.

1. Introduction

[2] Oxidation chemistry cleanses the atmosphere of chemical emissions from Earth's surface, establishes the global ozone balance, and influences climate change. It is dominated by the hydroxyl radical, OH, but also involves the hydroperoxyl radical, HO_2. OH and HO_2, together called HO_x, are highly reactive atmospheric constituents that have a large impact on the atmospheric chemistry by

[1]Department of Meteorology, Pennsylvania State University, University Park, Pennsylvania, USA.
[2]Now at Rosenstiel School of Marine and Atmospheric Sciences, University of Miami, Miami, Florida, USA.
[3]Science Directorate, NASA Langley Research Center, Hampton, Virginia, USA.
[4]School of Earth and Atmospheric Sciences, Georgia Institute of Technology, Atlanta, Georgia, USA.
[5]Earth Observing Laboratory, National Center for Atmospheric Research, Boulder, Colorado, USA.
[6]Department of Chemistry and Department of Earth and Planetary Science, University of California, Berkeley, California, USA.
[7]Graduate School of Oceanography, University of Rhode Island, Narragansett, Rhode Island, USA.
[8]Division of Engineering and Applied Sciences, California Institute of Technology, Pasadena, California, USA.
[9]NASA Ames Research Center, Moffett Field, California, USA.
[10]Department of Chemistry, University of California, Irvine, California, USA.
[11]National Suborbital Education and Research Center, University of North Dakota, Grand Forks, North Dakota, USA.

0148-0227/08/2007JD009166

influencing the removal of gases emitted into the atmosphere and the production of ozone and ultrafine aerosol particles.

[3] The basics of HO_x photochemistry have frequently been described [see, e.g., *Jaeglé et al.*, 2000]. The abundance of OH and HO_2 is primarily influenced by the HO_x production rate, the amount of NO_x ($NO_x = NO + NO_2$), and to some extent the types of hydrocarbons [*Jaeglé et al.*, 2000; *McKeen et al.*, 1997; *Singh et al.*, 1995, 2003]. In polar regions during springtime, halogen chemistry can influence HO_x and the HO_2/OH ratio in both the marine boundary layer [*Bloss et al.*, 2007] and the stratosphere [*Hanisco et al.*, 2002].

[4] HO_x has a number of sources: photolysis of ozone (O_3) followed by a reaction of $O(^1D)$ with H_2O, photolysis of formaldehyde (HCHO), nitrous acid (HONO), hydrogen peroxide (H_2O_2), methylhydroperoxide (CH_3OOH), and acetone ($CH_3C(O)CH_3$), as well as reactions between O_3 and alkenes. Its destruction is thought to be controlled by the relatively few type reactions: $HO_2 + HO_2$, $HO_2 + OH$, $HO_2 + RO_2$, and $OH + NO_2$.

[5] The NO_x abundance determines which reactions are the primary HO_x loss. At low NO_x, radical-radical reactions (particularly $HO_2 + HO_2$ and $HO_2 + RO_2$) dominate the loss of HO_x. As NO_x increases, $HO_2 + NO \rightarrow OH + NO_2$ shifts the partitioning of HO_x toward OH so that the $HO_2 + OH$ reaction begins to contribute significant to the loss. At high NO_x, direct reaction of OH with NO_2 to form HNO_3 becomes the primary loss. As a result, for fixed HO_x production ($P(HO_x)$), OH first increases until NO_x reaches a few ppbv and then decreases as a function of NO_x, while HO_2 remains roughly unchanged until NO_x reaches values for which $OH + NO_2 + M \rightarrow HNO_3 + M$ is the dominant loss and then decreases even faster than OH as NO_x continues to increase. As $P(HO_x)$ increases, the peak OH is higher and shifted to greater NO_x values [*McKeen et al.*, 1997]. Under high NO_x conditions, HO_x has a heightened sensitivity to HO_x sources [*Olson et al.*, 2006]. Thus, uncertainties in observations and reaction kinetics of HO_x precursors have a much more pronounced impact on modeled HO_x at high NO_x conditions compared to lower NO_x conditions.

[6] Reactions of OH with carbon monoxide (CO) and volatile organic compounds (VOCs) lead to the formation of HO_2 and organic peroxy radicals (RO_2). This conversion of OH is rapid. The inverse of the OH lifetime, the reaction frequency, which is usually called the OH reactivity, is typically 1 s^{-1} in clean environments near the surface, about 0.2–0.4 s^{-1} in the upper troposphere, and 5–100 s^{-1} in polluted urban environments. At the same time, HO_2 reacts with NO, producing O_3, or with O_3, destroying O_3, and in the process recreates OH. This cycle between OH and HO_2 is at times faster than the production and loss of HO_x. The reaction of RO_2 and NO leads to the formation of HO_2 and NO_2. The exact photochemistry that occurs depends mainly on the HO_x production ($P(HO_x)$), NO_x, the OH reactivity, and the yield of HO_2 and RO_2 from hydrocarbon oxidation [*Kleinman et al.*, 2002]. Understanding HO_x sources, sinks, and cycling is essential to develop predictive capability of pollution's influence on the atmosphere's oxidation capacity.

[7] The ratio of HO_2/OH is an important indicator of the HO_x cycling between OH and HO_2. A steady state expression for HO_2/OH comes from assuming that OH is in steady state:

$$\frac{[HO_2]}{[OH]} = \frac{k_{OH}}{(k_{NO+HO_2}[NO] + k_{O_3+HO_2}[O_3]) + P(OH)_{primary}/[HO_2]} \quad (1)$$

where $P(OH)_{primary}$ is the OH production rate from either photolysis of long-lived atmospheric constituents or from reactions of O_3 with alkenes; ($k_{NO+HO2}[NO] + k_{O3+HO2}[O_3]$) represents the cycling reaction frequency of HO_x from HO_2 to OH; and k_{OH} is the OH reactivity with all OH reactants, whether they are HO_x cycling or HO_x terminating reactions. We use the definition for primary OH sources to be those that are independent of local HO_x [*Jaeglé et al.*, 2001]. Typically the photolysis of O_3 followed by $O(^1D) + H_2O$ is the most important OH primary source, although the photolysis of HONO, H_2O_2, and CH_3OOH can also be important.

[8] For many atmospheric environments, the primary production, $P(OH)_{primary}$, and the terminating OH reaction rates are much smaller than the rate of reactions that cycle HO_x between OH and HO_2 and can be ignored. However, for the free troposphere between 2 km and 8 km in INTEX-A, the fraction of OH production by $P(OH)_{primary}$ is as often larger than OH production by HO_x cycling, ranging from 0.1 to 0.9 of total OH production, and cannot be ignored.

[9] Because HO_x photochemistry is sufficiently fast, comparisons with box models test the understanding of HO_x photochemistry. While scatterplots of measurements and model calculations are useful, examining the ratio of observed-to-modeled OH and HO_2 as a function of important variables provides even more information. The analyses of airborne tropospheric HO_x measurements from several different studies have been published [e.g., *Wennberg et al.*, 1998; *Crawford et al.*, 1999; *Brune et al.*, 1998, 1999; *Tan et al.*, 2001a; *Olson et al.*, 2004, 2006]. When all of the studies are taken together, we can reach the conclusion that HO_x photochemistry is generally understood and the results from last several missions are generally consistent, but that important large differences remain for some environments and conditions.

[10] Although the current agreement between measured and modeled HO_x is generally very good, there are specific environmental conditions where the agreement is weaker. Considering the critical role of HO_x in the production of secondary pollutants and the role of OH in the troposphere's oxidation capacity, further investigation into the causes of these differences is crucial. Emerging from previous HO_x studies are a set of conclusions: (1) HO_2, and thus calculated ozone production, is greater than model predictions at larger NO values for many tower-based studies and some aircraft studies, even though this discrepancy has been almost eliminated for two previous aircraft studies by reanalyses that more fully account for HO_x precursors and have updated reaction rate coefficients and products [*Olson et al.*, 2006]; (2) HO_2 and OH are larger than model predictions at high solar zenith angles, as in the Subsonic Assessment: Ozone and Nitrogen Oxide Experiment (SONEX) [*Brune et al.*, 1999], although the overtone photolysis of HO_2NO_2 could partly explain the discrepancy

[*Murphy et al.*, 2004]; (3) the evidence for heterogeneous influence on HO_x is still inconclusive, although some studies have provided evidence for significant removal in clouds [*Olson et al.*, 2006]; (4) even with highly constraining measurement suites, OH and HO_2 can be either significantly larger or smaller than model predictions in different environments and on different missions; whether this variation in agreement is due to unmeasured atmospheric constituents, instrumental drifts and changes, or differences in models, or a combination of all three, is not known; and (5) agreement of OH and HO_2 measured by different instruments has been inconsistent from comparison to comparison and for individual instrument in different environments [*Eisele et al.*, 2001, 2003; *Ren et al.*, 2003].

[11] This paper presents HO_x observation results and a steady state modeling analysis of fast photochemistry using measurements made during the INTEX-A campaign. The HO_x results from INTEX-A are compared to those from previous campaigns and to results for other related measurements from INTEX-A. Analyses of these comparisons provide the characteristics that uncertain or unknown chemistry must have in order to resolve discrepancies between measured and modeled HO_x that were observed in INTEX-A.

2. Experiment and Model Description

2.1. OH and HO_2 Measurements

[12] The OH and HO_2 radicals were measured with the Penn State ATHOS (Aircraft Tropospheric Hydrogen Oxides Sensor). ATHOS detects OH and HO_2 with laser-induced fluorescence (LIF). The technique uses a pump-down technique often called the fluorescent assay by gas expansion (FAGE) originally developed by *Hard et al.* [1984]. A detailed description of the ATHOS instrument can be found elsewhere [*Faloona et al.*, 2004]; here an abbreviated description of ATHOS is given.

[13] The air sample is drawn into a low-pressure chamber through a pinhole inlet (1.5 mm) with a vacuum pump. The pressure of the detection chamber varied from 12 to 3 hPa from 0 to 12 km altitude. As the air passes through a laser beam, OH is excited by a spectrally narrowed laser with a pulse repetition rate of 3 kHz at one of several ro-vibronic transition lines near 308 nm ($A^2\Sigma - X^2\Pi$, $v' = 0 \leftarrow v'' = 0$). Collisional quenching of the excited state is slow enough at the chamber pressure that the weak OH fluorescence extends beyond the prompt scattering (Rayleigh and wall scattering) and is detected with a time-gated microchannel plate (MCP) detector. HO_2 is measured by reaction with NO followed by the LIF detection of OH. The OH and HO_2 detection axes are in series: OH is detected in the first axis and HO_2 in a second axis as reagent NO (>99%, Matheson, Twinsburg, OH, purified through Ascarite) is added to the flow between the two axes. The OH fluorescence signal is detected 60 ns after the laser pulse has cleared in the detection cells and is recorded every 0.2 s. The laser wavelength is tuned on and off resonance with an OH transition every 10 s, resulting in a measurement time resolution of 20 s. The OH fluorescence signal is the difference between on-resonance and off-resonance signals.

[14] The instrument was calibrated both in the laboratory and during the field campaign. Different sizes of pinholes were used in the calibration to produce different detection cell pressures. Monitoring laser power, Rayleigh scattering, and laser line width maintained this calibration in flight [*Faloona et al.*, 2004]. For the calibration, OH and HO_2 were produced through water vapor photolysis by 185 nm light. Absolute OH and HO_2 mixing ratios were calculated by knowing the 185 nm flux, which is determined with a Cs-I phototube referenced to a NIST-calibrated photomultiplier tube, the H_2O absorption cross section, the H_2O mixing ratio, and the exposure time of the H_2O to the 185 nm light. The absolute uncertainty is estimated to be a factor of 1.32 for both OH and HO_2, at the 2σ confidence level. The uncertainty in measured HO_2/OH ratios is less, about ±15% at the 2σ confidence level, as determined from the precision of repeated simultaneous OH and HO_2 calibrations combined with estimated uncertainties of known factors affecting the relative OH and HO_2 measurements. The 2σ precisions for a 1-min integration time during this campaign were about 0.01 pptv for OH and 0.1 pptv for HO_2. Further details about the calibration process may be found elsewhere [*Faloona et al.*, 2004].

[15] Recently we revised our values for OH and HO_2 for the NASA missions TRACE-P, INTEX-A, and INTEX-B because of a problem with the ATHOS absolute calibration. The problem was related to an error in the calibration of our primary standard: a photomultiplier tube (PMT), which we use to measure the photon flux of a mercury lamp in our OH generator. The revised numbers are factor of 1.64 higher. Missions earlier than TRACE-P were unaffected. The conclusions of a few papers already published concerning these missions will need to be revisited to see if the ATHOS calibration change affects them.

2.2. Other Measurements on the DC-8

[16] The payload of the DC-8 and the measured chemical species and parameters are briefly described by *Singh et al.* [2006]. A large suite of atmospheric constituents were measured in INTEX-A, including CO, O_3, H_2O, reactive nitrogen (NO, NO_2, HNO_3, HO_2NO_2, PAN), more than 50 VOCs and oxygenated VOCs (OVOCs), and important HO_x precursors such as peroxides (H_2O_2 and CH_3OOH) and aldehydes (HCHO and acetaldehyde). Spectral radiometers allowed direct measurement of actinic flux used to derive key photolysis frequencies.

[17] The measurements of NO_2 were made with laser-induced fluorescence [*Thornton et al.*, 2000] and measurements of NO were made with a TECO Model 42C NO-NO_x analyzer run in an NO only mode, which had a precision of 50 pptv with 1-min time integration. Because of this large NO limit of detection, concentrations of NO were predicted using the steady state model and measured NO_2. A linear regression of the NO obtained from measurements and the model is the equation: $NO_{modeled} = 0.92 \times NO_{measured} - 16$ pptv, with $R^2 = 0.76$ and where, $NO_{modeled}$ was calculated in the model using observed NO_2, O_3, NO_2 photolysis frequency, and modeled HO_2 and RO_2. This agreement gives confidence that NO from the model, rather than measurements, can be used at low NO, where the NO measurement is noisy and may have a small offset, and at high NO, where NO obtained from measurements and from the model are in excellent agreement.

2.3. Model Description

[18] A zero-dimensional, time-dependent photochemical box model developed at NASA Langley Research Center was used to calculate OH, HO_2 and other reactive intermediates. The model has been described in detail in several previous studies [e.g., *Crawford et al.*, 1999; *Olson et al.*, 2004]. The modeling approach is based on the assumption of a diurnal steady state. For a suite of simultaneous measurements of input species at a given point in time, the model integrates to find a self-consistent diurnal cycle for the computed species based on constraining selected species to the measurements. Computed concentrations at the point in time of measurement are then used as the instantaneous model results. This approach ensures that all computed species are in equilibrium with the diurnal process, which is crucial for species with lifetimes too long for simple instantaneous steady state assumptions. For input, model calculations use observations from the 1-min merged data set available on the INTEX-A public data archive (ftp://ftp-air.larc.nasa.gov/pub-air/INTEXA/). The minimum set of input constraints includes observations of O_3, CO, NO_2, NMHC, acetone, methanol, temperature, H_2O (dew/frost point), pressure, and photolysis frequencies. For this analysis, analyzed data were limited to solar zenith angles (SZA) between 0° and 85°.

[19] In addition to the required constraints described above, the model has the option to include additional constraints when measurements are available for hydrogen peroxide (H_2O_2), methyl hydrogen peroxide (CH_3OOH), nitric acid (HNO_3), and peroxy acetyl nitrate (PAN). If unavailable, these atmospheric constituents are calculated by the model based on diurnal steady state. While each of the H_2O_2, CH_3OOH, HNO_3, or PAN measurements were missing 20–35% of the measurement time, all of the H_2O_2, CH_3OOH, HNO_3, and PAN measurements were simultaneously missing less than 2% of the measurement time. Model calculations taking advantage of these additional constraints are referred to as "constrained." All model results discussed in this paper are taken from the constrained model calculations unless explicitly stated otherwise. For the purpose of model-to-measurement comparisons, an unconstrained version was also run for which none of the additional constraints were exercised; that is, the peroxides, PAN, and HNO_3 were always predicted.

[20] Neither the unconstrained model nor the constrained model was constrained to the measured HCHO, just as was done for previous campaigns. Rather, HCHO is used as an additional species for which comparisons between the observations and model may provide insight into current knowledge of photochemical cycling. Evidence suggests that the differences in the observed and modeled HCHO do not significantly influence the comparisons between observed and modeled OH, HO_2, and HO_2/OH [*Olson et al.*, 2004; A. Fried et al., Role of convection in redistributing formaldehyde to the upper troposphere over North America and the North Atlantic during the summer 2004 INTEX campaign, submitted to *Journal of Geophysical Research*, 2007].

[21] In order to maximize the number of points available for modeling, nonmethane hydrocarbons were interpolated between consecutive grab samples, which were collected throughout each flight at a frequency of every 4–5 min during horizontal flight legs and every 1–2 min during ascents and descents. Similarly, acetone and methanol were interpolated between adjacent measurements to fill data gaps.

[22] As in previous studies, photolysis frequencies were based on spectroradiometer measurements [*Shetter and Muller*, 1999]. The diurnal profile for each photolysis frequency is based on clear-sky model calculations using a Discrete Ordinate Radiative Transfer (DISORT) eight-stream implementation of the NCAR Tropospheric Ultraviolet Visible (TUV) radiative transfer code [*Madronich and Flocke*, 1998]. The clear-sky diurnal variation from TUV is then normalized to measured photolysis frequencies at the time of observation. Unmeasured photolysis frequencies $J[NO_3 + h\nu \rightarrow NO + O_2]$, $J[NO_3 + h\nu \rightarrow NO_2 + O]$, and $J[N_2O_5 + h\nu \rightarrow NO_2 + NO_3]$ were first calculated for clear sky conditions and then corrected for ambient cloud conditions on the basis of the ratio of measured-to-calculated photolysis frequency of NO_2.

[23] The uncertainties in the modeled OH and HO_2 are based on the combined uncertainties of the kinetic rate coefficients, the measured chemical concentrations, and the measured and calculated photolysis frequencies. The uncertainties in the model due to kinetic rate constant uncertainties were estimated with a Monte Carlo approach, as in, for example, the works by *Thompson and Stewart* [1991] or *Carslaw et al.* [1999]. The 2σ uncertainty was estimated to be ±59% for OH and ±53% for HO_2 in the upper troposphere (8–12 km), about ±40% for OH and 45% for HO_2 in the middle troposphere (2–8 km), and ±28% for OH and ±24% for HO_2 in the boundary layer, on the basis of median conditions observed for INTEX-A.

3. Observations, Model Results, and Comparisons

[24] During INTEX-A, the DC-8 encountered a variety of air masses. These include air masses that were influenced by anthropogenic pollution, biomass burning, convection, the stratosphere, and mixtures of these different types. These plumes are often distinguishable by their characteristic composition. Anthropogenic pollution contains high CO, anthropogenic hydrocarbons, and often water vapor. Biomass burning plumes can be distinguished from anthropogenic pollution by high HCN and acetonitrile. Convection plumes can be distinguished by high NO_x/NO_y ratios, water vapor, ultrafine particles, and O_3. Stratosphere-influenced air can be defined as air having O_3 greater than ~100 ppbv, CO less than ~100 ppbv, water vapor less than 200 ppmv, and low hydrocarbon levels. The different composition of these air masses provides an excellent opportunity to examine HO_x photochemistry for a range of conditions.

3.1. HO_x Observations and Comparison With the Model Calculations

[25] Altitude profiles of observed OH and HO_2 spanned from a few hundred meters above the surface to almost 12 km (Figure 1). Median OH was relatively constant at 0.25 pptv from altitudes near the surface to 6 km, but then increased with altitude above 6 km, achieving a maximum of about 0.86 pptv at 12 km. HO_2 decreased as the altitude increased, with a maximum median of ~30 pptv near the

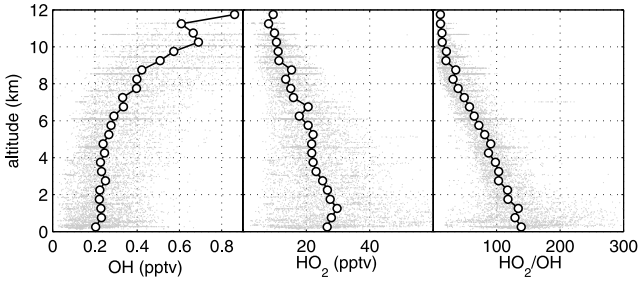

Figure 1. Observed OH and HO_2 mixing ratios and HO_2/OH ratio as a function of altitude during INTEX-A. Small dots are the 1-min averaged data; the linked circles denote median values in 0.5 km altitude bins.

surface and a minimum median of ~8 pptv at the highest altitude. The greatest HO_2, almost 60 pptv, was observed just above the surface over the central United States. The median HO_2/OH ratio dropped from 140 near the surface to 12 above 10 km, driven by both the decrease in HO_2 and the increase in OH with altitude. At low altitudes, the spread in HO_2/OH is quite large, from 20 to 300, indicating a wide range of air composition there.

[26] Overall comparisons of observed and modeled OH and HO_2 show that on average observed OH and HO_2 generally agree with modeled OH and HO_2. However, for less HO_x, observed OH and HO_2 generally exceeded the modeled OH and HO_2 (Figure 2). Because less HO_2 was mostly observed at high altitudes, these plots suggest that the behavior of HO_x should be investigated as a function of altitude.

[27] Detailed statistics characterize the behavior of the observed-to-modeled ratios as a function of altitude for OH, HO_2, and HO_2/OH (Table 1). The "% within ±32%" is the percentage of model values that are the same as the measured values to within the measurement 2σ uncertainty of a factor of 1.32; the "% mod > obs × 1.32" is the percentage of model values greater than 1.32 times the observed values; and the "% mod < obs/1.32" is the percentage of model values less than the observed values divided by 1.32. Although the model also has uncertainty, using the 2σ measurement uncertainty provides a good indication of the differences between the observed and modeled values and where they are occurring.

[28] OH is well predicted by the model at all altitudes except in the boundary layer where OH is underpredicted, with roughly half of the modeled values falling within the 2σ measurement uncertainty (±32%) (Table 1 and Figure 3). For a smaller number of observations, OH is underpredicted in the continental boundary layer and in a few plumes at higher altitudes. The underprediction in the boundary layer correlates strongly with isoprene and will be discussed in detail later. HO_2 is generally well predicted below 8 km with a slight underprediction, but is significantly underpredicted above 8 km (Table 1 and Figure 4). Large underpredictions of HO_2 in the upper free troposphere above 8 km are highly correlated with NO and will be discussed in detail later.

[29] The HO_2/OH ratio is generally well predicted throughout the troposphere (Table 1 and Figure 5). Below 8 km, the median observed-to-modeled ratio is less than 1.5. Median values of the HO_2/OH observed-to-modeled ratio are biased slightly high because it tends to be slightly underpredicted for HO_2. Above 8 km, the large differences in the observed-to-modeled HO_2/OH are driven more by the differences in observed-to-modeled HO_2 than they are in the differences between the observed-to-modeled OH.

[30] There are two possible explanations for the general observed and modeled agreement in some cases but not in others. The first explanation is that OH and HO_2 measurements are affected by large interferences in some environments. ATHOS has been extensively tested for interferences for both OH and HO_2 [*Ren et al.*, 2004]; no interference that could be responsible for these measurements has been found. A second explanation is that uncertainties or unknowns in the chemistry are responsible for at least some of the observed-to-modeled discrepancies. In the absence of evidence that the absolute calibration is not good to within the stated ±32% at the 2σ confidence level, we will assume that all the discrepancies are caused by uncertain or unknown chemistry and will at least characterize the effects of the unknown chemistry, even if we cannot identify it by name.

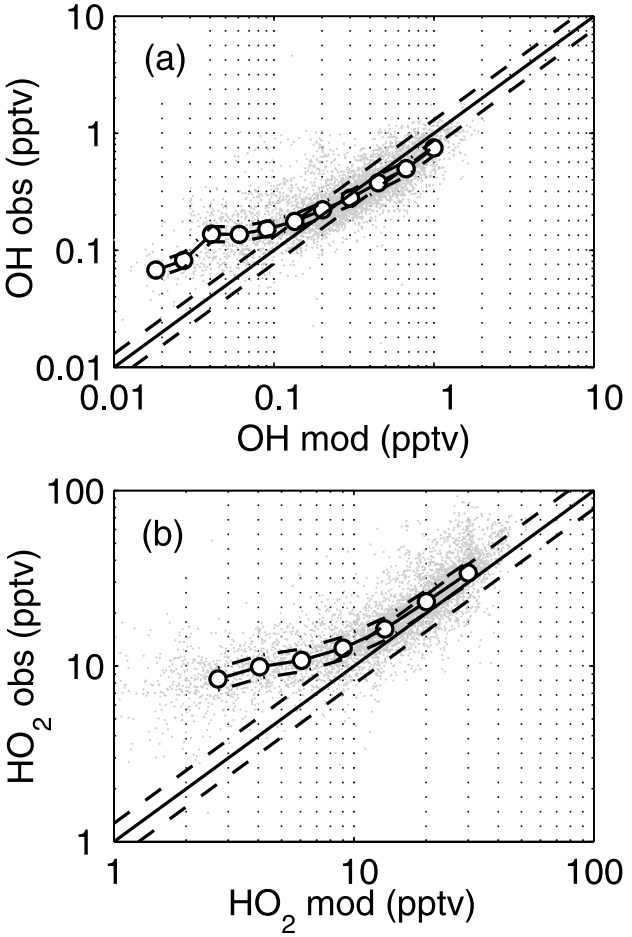

Figure 2. Comparison of observed and modeled (a) OH and (b) HO_2 in INTEX-A. The straight solid lines indicate the 1:1 lines, the dashed lines indicate the 1-σ uncertainty in the model (±30% for OH and ±27% for HO_2, the maximum uncertainties estimated for the 8–12 km altitude range), the solid line with circles are the median values for the observations, and the dash-dotted lines are the 1-σ uncertainty for the observations (±16%).

Table 1. Statistics for HO_x Observed-to-Modeled Ratios

	Overall	0–2 km	2–8 km	8–12 km
		OH Obs/Mod		
Median (mean)	0.95 (1.24)	1.00 (1.54)	0.92 (1.05)	0.98 (1.25)
% within ±32%	52%	47%	58%	50%
% mod < obs/1.32 below 2σ	23%	34%	16%	24%
% mod > obs × 1.32	25%	19%	26%	26%
		HO_2 Obs/Mod		
Median (mean)	1.28 (2.87)	1.37 (1.57)	1.13 (2.10)	2.05 (5.49)
% within ±32%	50%	41%	74%	19%
% mod < obs/1.32 below 2σ	46%	56%	20%	79%
% mod > obs × 1.32	4%	3%	6%	2%
		HO_2/OH Obs/Mod		
Median (mean)	1.33 (1.68)	1.26 (1.26)	1.20 (1.24)	2.20 (2.88)
% within ±32%	40%	40%	55%	13%
% mod < obs/1.32 below 2σ	50%	44%	36%	83%
% mod > obs × 1.32	10%	16%	9%	4%

3.2. Comparisons of Observed and Modeled HO_x With Previous Studies

[31] ATHOS has measured OH and HO_2 during several recent field studies. The three most recent are the Pacific Exploratory Mission Tropics–B (PEM-TB) [*Raper et al.*, 2001], TRACE-P [*Jacob et al.*, 2003], and INTEX-A [*Singh et al.*, 2006]. PEM-TB was conducted in the tropical Pacific, usually in relatively clean air. In contrast, TRACE-P was conducted off the coast of Asia in air that was often quite polluted. Both occurred in spring and provide an interesting contrast to INTEX-A, which was conducted either over the continental US or over the Atlantic Ocean downwind of it in summer. Comparisons of these three studies are particularly compelling because ATHOS was used to measure OH and HO_2 in all three and OH, HO_2, and HCHO for several previous missions including PEM-TB and TRACE-P were recently recalculated using the same photochemistry and constraints as were used for INTEX-A [*Olson et al.*, 2006].

[32] The behavior of atmospheric constituents that interact with OH and HO_2 is quite different for the three studies (Figure 6). Carbon monoxide (CO) is similar for TRACE-P and INTEX-A, except at lower altitudes where Asian pollution observed during TRACE-P contained much more CO than North American pollution observed during INTEX-A. CO in both northern hemisphere studies are roughly twice that observed in PEM-TB. O_3 is similar for INTEX-A and TRACE-P up to ~8 km, where O_3 in INTEX-A continues to increase. O_3 in PEM-TB is less than

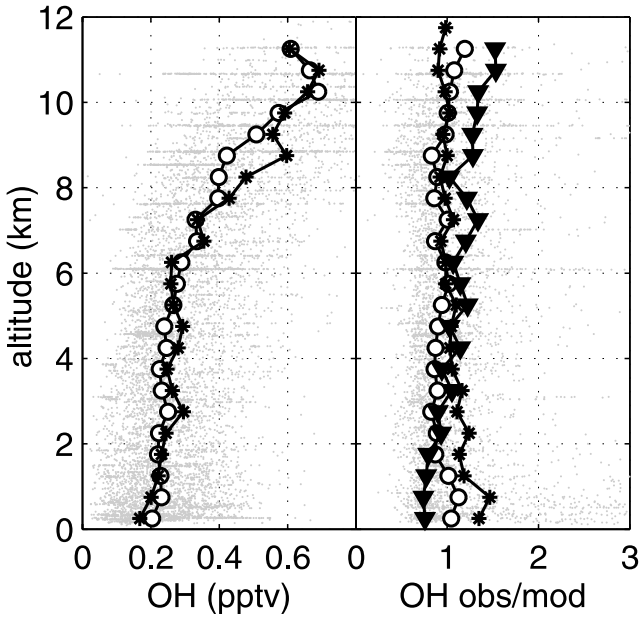

Figure 3. Comparison of the median vertical profiles of (left) measured (circles) and modeled (stars) OH in INTEX-A and (right) measured-to-modeled OH ratios in INTEX-A (circles), TRACE-P (stars) and PEM Tropics B (triangles). Individual INTEX-A 1-min measurements are shown (gray dots). The lines in the right diagram represent the median values of 1-min time-resolved obs/mod ratios.

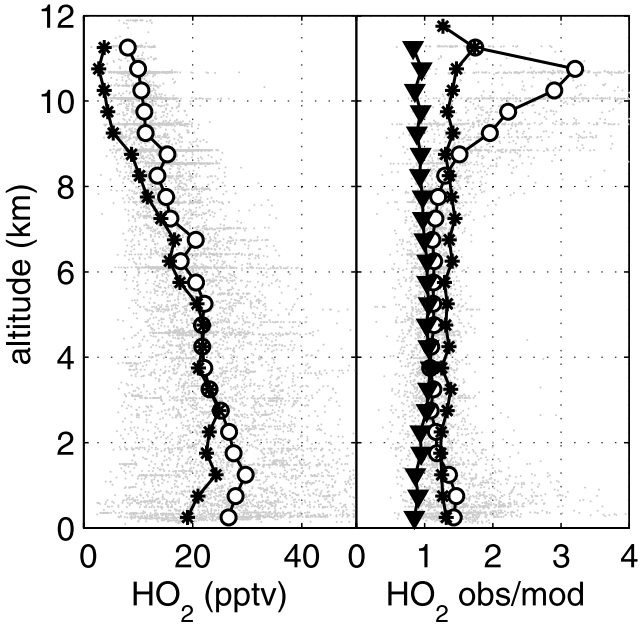

Figure 4. Comparison of the median vertical profiles of (left) measured (circles) and modeled (stars) HO_2 in INTEX-A and (right) measured-to-modeled HO_2 ratios in INTEX-A (circles), TRACE-P (stars) and PEM Tropics B (triangles). Individual INTEX-A 1-min measurements are shown (gray dots). The lines in the right diagram represent the median values of 1-min time-resolved obs/mod ratios.

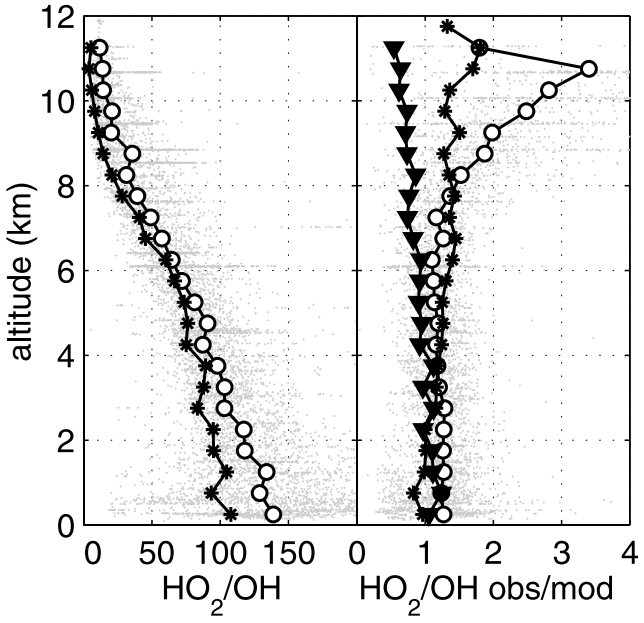

Figure 5. Comparison of the median vertical profiles of (left) measured (circles) and modeled (stars) HO_2/OH in INTEX-A and (right) measured-to-modeled HO_2/OH in INTEX-A (circles), TRACE-P (stars) and PEM Tropics B (triangles). Individual INTEX-A 1-min measurements are shown (gray dots). The lines in the right diagram represent the median values of 1-min time-resolved obs/mod ratios.

half these other two studies. The greatest differences were with NO_x. Observed NO_x was more than four to five times larger during INTEX-A than during TRACE-P and more than an order of magnitude larger than during PEM-TB. These differences are most pronounced above 8 km, where NO_x during INTEX-A was sometimes more than 1.5 ppbv.

[33] The conditions among the three studies are quite different. It is therefore instructive to compare not only the absolute values of OH, HO_2, and the HO_2/OH ratio, but also the ratios of the measured-to-modeled OH, HO_2, and HO_2/OH ratio for the three studies. These are plotted as a function of the controlling environmental factors such as altitude (Figures 3, 4, and 5) and NO (Figure 7).

3.2.1. Comparison as a Function of Altitude

[34] As stated in section 2.1, the observed OH and HO_2 mixing ratios in INTEX-A and TRACE-P have been increased by a factor of 1.64 because of a calibration correction. The median observed-to-modeled OH ratio in INTEX-A is similar to that observed in TRACE-P (Figure 3). On the other hand, the median observed-to-modeled OH ratio in INTEX-A is different from that in PEM-Tropics B, where it was ~0.7 only below 1 km; above that, the median observed-to-modeled OH ratio increases monotonically to 1.3 at 12 km [*Tan et al.*, 2001a; *Olson et al.*, 2001].

[35] The observed-to-modeled HO_2 ratio has quite different behavior as a function of altitude in INTEX-A compared to that in either TRACE-P or PEM-TB (Figure 4). For altitudes between 2 km and below 8 km, the observed-to-modeled HO_2 ratio is similar for INTEX-A, TRACE-P and PEM-TB, all being around 1. In all three studies, the ratio changed little over this altitude range. The large increase in the observed-to-modeled HO_2 ratio above 8 km is quite different from either TRACE-P or PEM-TB. This difference is consistent with the substantially greater NO_x observed above 8 km during INTEX-A than during the other two studies (Figure 6). For altitudes below 2 km, the observed-to-modeled HO_2 is about 1.5 for INTEX-A, 1.3 for TRACE-P, and 1.0 for PEM-TB.

[36] Enhanced NO_x was also observed during SUCCESS (Subsonic aircraft; Contrails and Clouds Effect Special Study), both in and out of aircraft exhaust plumes. The ability to conclusively analyze the observations made in the exhaust plumes was limited by sampling with insufficient resolution to appropriately model nonlinear HO_x-NO_x interactions [*Olson et al.*, 2006]. For the SUCCESS observations not impacted directly by aircraft exhaust, a tendency for significant deviation between modeled and observed HO_2 remains [*Brune et al.*, 1998]. However, the lack of measurements of several potentially important HO_x precursors limits what can be said with confidence about the underpredicted HO_2 that was observed during SUCCESS.

[37] Similar behavior was observed during TRACE-P, where a subset of the TRACE-P observations in stratospherically influenced air above 9 km near 35°N had an observed-to-modeled HO_2 ratio of 2.6 [*Olson et al.*, 2004].

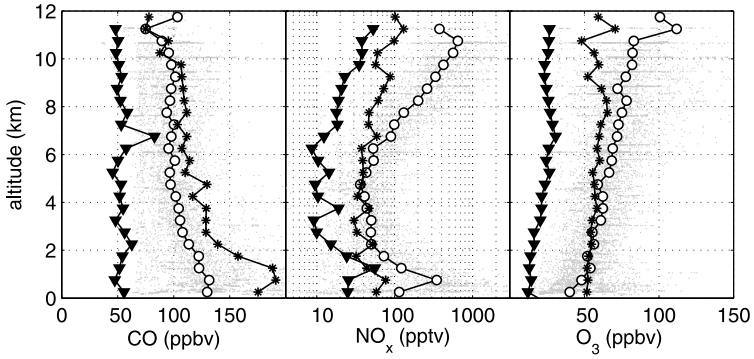

Figure 6. Comparisons of the median altitude profiles for atmospheric constituents in PEM Tropics B (triangles), TRACE-P (stars), and INTEX-A (circles) for (left) CO, (middle) NO_x, and (right) O_3. Individual 1-min measurements in INTEX-A are shown as gray points. For INTEX-A, NO_x is the sum of measured NO_2 and calculated NO.

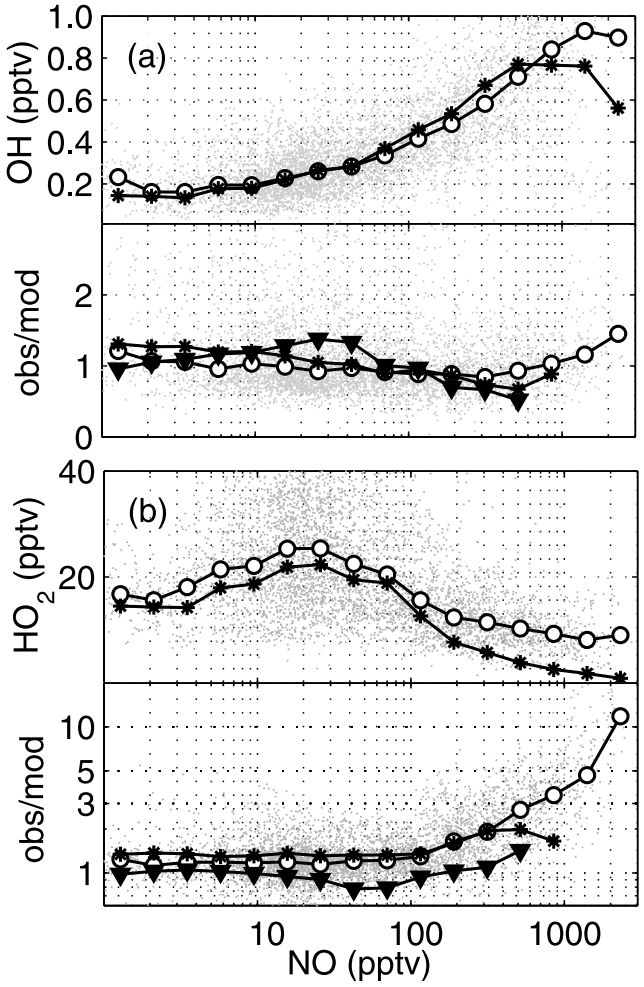

Figure 7. Comparison of NO dependence for (a) OH and (b) HO_2 of (top) measured (circles) and modeled (stars) values and (bottom) measured-to-modeled ratios in INTEX-A (circles), TRACE-P (stars) and PEM Tropics B (triangles). Individual INTEX-A 1-min measurements are shown (gray dots). Concentrations of NO calculated in the model are used. All lines show the median profiles.

However, unlike TRACE-P, where the observed-to-modeled ratio was around 1 in stratospherically influenced air, 92% of the INTEX-A observations with an observed-to-modeled HO_2 ratio significantly greater than 1 were in tropospheric air that was not obviously influenced by the stratosphere. Thus this INTEX-A result appears to be unprecedented.

[38] The behavior of the observed-to-modeled HO_2/OH ratio is different in all three studies (Figure 5). For PEM-TB, the observed-to-modeled ratio near 1 at lower altitudes, but above 6 km begins to decrease, reaching 0.6 near 12 km. For TRACE-P, the opposite occurs; the ratio is slightly below 1 at low altitudes, but then increases to about 1.4 above 7 km. The INTEX-A observed-to-modeled HO_2/OH ratios greater than 2 at altitudes above 8 km were not observed in the other studies. The large increase in the observed-to-modeled HO_2/OH ratio at altitudes above 8 km is mainly driven by the underpredicted HO_2.

3.2.2. Comparison as a Function of NO

[39] Both OH and HO_2 qualitatively show the expected behavior as a function of NO for INTEX-A (Figure 7), although important quantitative differences occur. For OH, the observed-to-modeled ratios for PEM-TB, TRACE-P, and INTEX-A are fairly constant with increasing NO.

[40] The observed-to-modeled HO_2 ratio increases from values below and near 1 to values more than 1 when NO is more than a few hundred pptv in all three studies, although the amount of change is different for the three studies. It is worth noting that the highest NO values were observed in the upper troposphere during INTEX-A, while the highest NO values were observed in boundary layer during TRACE-P.

3.3. HO_x Budget Calculations

[41] Examining the HO_x production and loss provides information about the balance between HO_x sources and sinks. The HO_x production consists of the production from the following processes: O_3 photolysis followed by the $O(^1D) + H_2O$ reaction, HCHO photolysis (the radical-producing pathway only), H_2O_2 photolysis, and the ozonolysis of alkenes. HO_x loss includes the OH reaction with

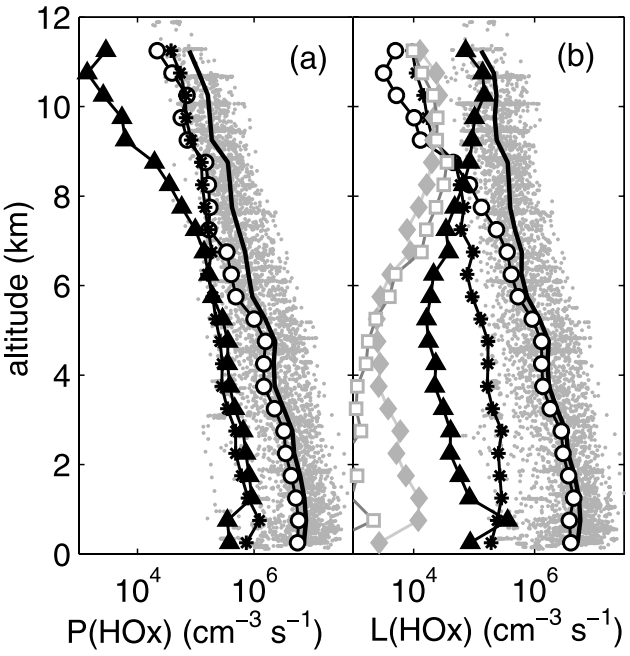

Figure 8. Vertical median profiles of (a) HO_x production, showing total production (thick line) and production from $O(^1D) + H_2O$ (circles), from HCHO photolysis (stars), and from H_2O_2 photolysis (triangles), and (b) HO_x loss rates, showing total loss rates (thick line) and loss rates due to $HO_2 + HO_2/RO_2$ (circles), due to $OH + HO_2$ (stars), due to $OH + NO_x$ (triangles), due to $OH + HNO_3$ (diamonds), and due to $OH + HO_2NO_2$ (squares) during INTEX-A. Small gray dots show the 1-min data for total HO_x production rate (Figure 8a) and total HO_x loss rate (Figure 8b). All the production and loss rates were calculated from the measurements, except for $RO_2 + HO_2$ where RO_2 levels were calculated in the model. The total production and loss rates are the sums of all production or loss terms.

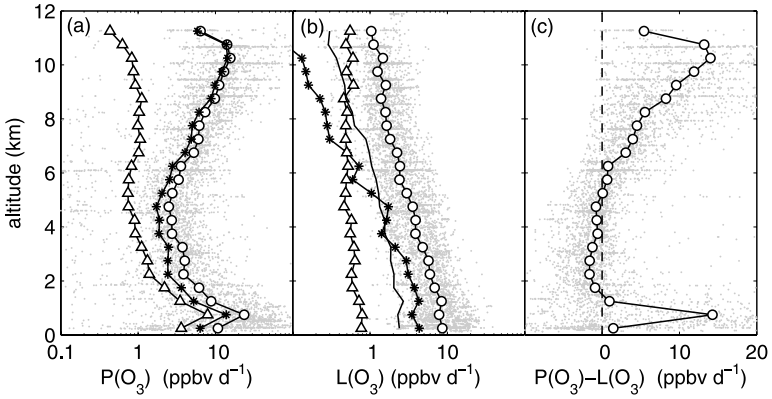

Figure 9. Vertical median profiles of (a) diurnal O_3 production rate, showing total production rates (circles) and production rates from HO_2 + NO (stars) and from RO_2 + NO (triangles) where RO_2 levels were calculated in the model; (b) O_3 loss rates, showing total loss rates (circles) and loss rates due to $O(^1D)$ + H_2O (stars), due to O_3 + OH (triangles), and due to O_3 + HO_2 (solid line); and (c) net O_3 production rate during INTEX-A. Small gray dots show the 1-min data for total O_3 production rate (Figure 9a), total O_3 loss rate (Figure 9b), and net O_3 production (Figure 9c).

NO_2 and the reactions among OH, HO_2 and RO_2. For this discussion, RO_2 was calculated by the box model.

[42] The main $P(HO_x)$ was the reaction $O^1D + H_2O$ below 7 km and the photolysis of HCHO above 7 km (Figure 8a). Photolysis of H_2O_2 contributed little to $P(HO_x)$. For the HO_x loss, HO_2-RO_2 self-reactions were the main processes below 8 km and the OH + NO_x reactions became the main loss processes above 8 km (Figure 8b).

3.4. Diurnal Average of Calculated Ozone Production

[43] The net calculated ozone production in the troposphere is given to a close approximation by

$$\begin{aligned} P(O_3)_{net} = P(O_3) - L(O_3) &= k_{NO+HO2}[NO][HO_2] \\ &+ \Sigma_i k_{NO+RO2i}[NO][RO_{2i}] - k_{OH+NO2+M}[M][NO_2][OH] \\ &- k_{O1D+H2O}\left[O\left(^1D\right)\right][H_2O] - k_{HO2+O3}[O_3][HO_2] \\ &- k_{OH+O3}[O_3][OH] \end{aligned} \quad (2)$$

where k_{NO+HO2}, $k_{NO+RO2i}$ $k_{OH+NO2+M}$, $k_{O1D+H2O}$, k_{HO2+O3}, and k_{OH+O3} are reaction rate coefficients. The diurnally averaged values of the calculated ozone production and loss terms come from the time-dependent model simulations. In order to determine the O_3 budget based on observed values of HO_x, the model was run with the computed diurnal profiles of OH and HO_2 scaled throughout the diurnal cycle to match the observed concentrations at the appropriate time of day. The resulting calculated O_3 production was mainly from the HO_2 + NO reaction, especially at altitudes greater than 5 km (Figure 9a). At altitudes around 10 km, the calculated O_3 production from RO_2 + NO accounted for less than 10% of the total. For the O_3 loss rate, O_3 photolysis followed by the $O(^1D)$ + H_2O reaction was the main O_3 loss process below 5 km, while O_3 reactions with OH and HO_2 became the main O_3 loss above 6 km because of low H_2O mixing ratios at these altitudes (Figure 9b).

[44] Net calculated ozone production with a median value of 8.4 ppbv d^{-1} was found for the lowest altitude (<1 km), while a median loss of 0.8 ppbv d^{-1} was found for the lower troposphere (1–5 km). For observations above 9 km, a median net O_3 production rate of 11.4 ppbv d^{-1} was calculated (Figure 9c). For the upper altitudes, the O_3 production drops to 4.5 ppbv d^{-1} when model predictions of HO_x are used rather than observed values. This significant difference underscores the importance of understanding the upper tropospheric HO_x discrepancies in the INTEX-A data. The important role of lightning NO_x is also emphasized by the large rates of net production in INTEX-A compared to previous campaigns. Calculated ozone production in the upper troposphere during TRACE-P was less than 1.5 ppbv d^{-1} [*Davis et al.*, 2003] and was ~0.5 ppbv d^{-1} during PEM-Tropics B [*Olson et al.*, 2001].

4. Discussion

[45] Two significant differences between observed and modeled HO_x become apparent in the INTEX-A data: underpredicted HO_2 above 8 km and underpredicted OH in the continental planetary boundary layer.

4.1. Underpredicted HO_2 Above 8 km Altitude

[46] Convection had a large impact on the atmospheric composition in this altitude range during INTEX-A [*Bertram et al.*, 2007], most notably with enhancements for lightning NO_x (Figure 6), but also for peroxides, HCHO, and sometimes other constituents. Above 8 km, more than 2/3 of the observations of HO_2 and HO_2/OH were greater than expected, while only a small number of OH observations were.

[47] Could this underpredicted HO_2 be an instrument artifact? An offset to the HO_2 signal would make HO_2 appear larger than it is. However, the observed-to-modeled HO_2 ratio is uncorrelated with observed HO_2, which varied from 3 pptv to 30 pptv above 8 km. In addition, no single offset HO_2 value can be found to improve the agreement between the observed and modeled HO_2. These results rule out a constant offset in the HO_2 signal. The only gas that is known to photolyze in the ATHOS laser beam to produce HO_2, but no OH, is formaldehyde, but the HCHO measured

in INTEX-A is orders of magnitude too small to produce the observed signals [*Ren et al.*, 2004].

[48] The large observed-to-modeled HO_2 ratio above 8 km is consistent with the underpredicted H_2O_2, but not consistent with observed pernitric acid (HO_2NO_2). If HO_2NO_2 were in steady state with HO_2 and NO_2, the calculated steady state value of HO_2 would need to be lower than even the modeled HO_2. This difference is consistent with the possibility of the termination reaction for OH that actually improves the model-to-observed comparison for HO_2NO_2 [*Kim et al.*, 2007].

[49] If the observed HO_2 is not an instrument artifact, then the underpredicted HO_2 indicates an additional unknown HO_x source or a reduced HO_x sink; the underpredicted HO_2/OH indicates either slower HO_x cycling from HO_2 to OH or faster HO_x cycling from OH to HO_2.

[50] Consider first the underprediction of HO_2. Either an additional unknown HO_x source or a reduced HO_x sink must be capable of improving the observed-to-modeled HO_2 agreement above 8 km without making the agreement worse at lower altitudes. Thus, the cause of HO_2 underprediction must be insignificant from 2 to 8 km and must have increasing importance from 8 to 11 km.

[51] If a reduced HO_x sink is the cause, then the error would need to be in the known termination reactions of OH with NO_2, NO, HNO_3, and HO_2NO_2 because they dominate above 8 km and are insignificant below 8 km (Figure 8). However, for terminal HO_x loss by reaction with NO_x to be the cause of the HO_2 underprediction, the HO_x loss rate by these reactions would have to be 5 to 8 times less than expected. This difference is well outside uncertainties for the measured reactants and reaction rate coefficients. Thus, a reduced HO_x sink is unlikely to be the cause of the HO_2 underprediction.

[52] If underpredicted HO_x production is the cause, then the error would need to result from either an error in the known HO_x sources or additional unknown HO_x sources. The known, equally dominant HO_x sources in the altitude region are O_3 photolysis followed by $O(^1D) + H_2O$ and HCHO photolysis. In order to bring modeled and observed HO_2 into agreement, an additional HO_x source of 1.5×10^6 molecules cm^{-3} s^{-1} is needed above 8 km. This amount is about 4 times larger than the known HO_x sources (Figure 8). Below 8 km, this source would need to decrease to less than $\sim 10^5$ molecules cm^{-3} s^{-1} at 6 km and below. It is worth noting that this increase with altitude of the needed additional HO_x source is similar to the observed increase in NO_x with increasing altitude (Figure 6).

[53] Can the HO_2 underprediction come from errors in a known source? The O_3 photolysis and HCHO photolysis are about equal HO_x sources above 8 km. The HO_x production rate from either one of them would need to be increased by a factor of 4 to 6 above 10 km. O_3 photolysis could not be low by that much at 10 km and still be consistent with the HO_x observed-to-modeled ratios below 10 km, where O_3 photolysis is the dominant HO_x source. This inconsistency rules out an error in O_3 photolysis as the cause of the HO_2 underprediction. Constraining the model to observed HCHO reduces the observed-to-modeled HO_2 ratio by less than 25% (Fried et al., submitted manuscript, 2007). The HCHO photolysis frequency is unlikely to be in error by the factor of 4 to 6 needed to bring the measured and modeled HO_2 into agreement, because there is good agreement between the photolysis frequency measurements and radiative transfer model results at all altitudes. It is important to note that the Fried et al. (submitted manuscript, 2007) study also observed a HCHO measurement/model discrepancy between 10 km and 12 km that scaled with NO, similar to the HO_2 discrepancy.

[54] Thus, unknown HO_x sources are the most likely cause of the HO_2 underprediction. One characteristic of the unknown source is that it correlates with NO. For the observed-to-modeled HO_2 ratio above 8 km, the HO_2 observed-to-modeled ratio = 0.004 x NO (in pptv) + 0.88 with $r^2 = 0.54$. In previous studies, it was assumed that the chemistry and HO_x sinks were understood and that the underpredicted HO_2 was due to missing HO_x sources that were emitted along with the NO [see, e.g., *Folkins et al.*, 1997; *Wennberg et al.*, 1998; *Jaeglé et al.*, 2000]. While we have been able to quantify the additional HO_x production that would be needed, to identify its altitude dependence, and to show a correlation with NO, we have not been able to identify this additional unknown HO_x source.

[55] A second issue is the underpredicted HO_2/OH ratio. This ratio indicates that reactions and reactants that cycle HO_x between OH and HO_2 are not being properly represented in the model. The HO_2/OH underprediction can be explained by either slower reactions of HO_2 with NO or faster OH reactions that cycle OH to HO_2. At these altitudes, the reaction frequency of $HO_2 + NO \rightarrow OH + NO_2$ is an order of magnitude faster than primary OH production (equation (1)). The reaction frequency for HO_2 + NO would need to be less than $^1/_2$ its calculated value; this difference is unlikely and inconsistent with many other studies. It is possible that other reactants with HO_2, such as BrO, are present, but their reactions with HO_2 would make HO_2/OH smaller, not larger. Thus, the underpredicted HO_2/OH ratio indicates the presence of unknown reactants or reactions with OH that cycle HO_x from OH to HO_2.

[56] In this case, the needed increase in the OH reactivity that cycles HO_x between OH and HO_2 is proportional to the observed-to-modeled HO_2/OH ratio. As a result, the needed additional OH reactivity is ~ 0.15 s^{-1} at 8 km, about $^1/_2$ of the calculated OH reactivity, and ~ 0.5 s^{-1} above 10 km, almost twice the calculated OH reactivity. Interestingly, the needed OH reactivity is roughly proportional to the increase in NO_x in that altitude range, suggesting that the convective processes that enhanced NO_x also yielded additional, unknown OH reactants.

[57] In the presence of greater NO, the differences in OH and HO_2 between the model constrained to observed H_2O_2, CH_3OOH, HNO_3, and PAN and the model unconstrained by these observations grows (Figure 10). This behavior indicates that the modeled OH and HO_2 are quite sensitive to the model constraints, especially above 8 km altitude where the NO was increasing. In this altitude region, the cycling of HO_2 due to NO dominates the production of OH and makes HO_x more sensitive to small differences in the constraints placed on the model photochemistry.

4.2. Underpredicted OH in the Continental Planetary Boundary Layer

[58] During INTEX-A, the observed-to-modeled OH ratio is frequently much greater than 1.0 below 2 km altitude in

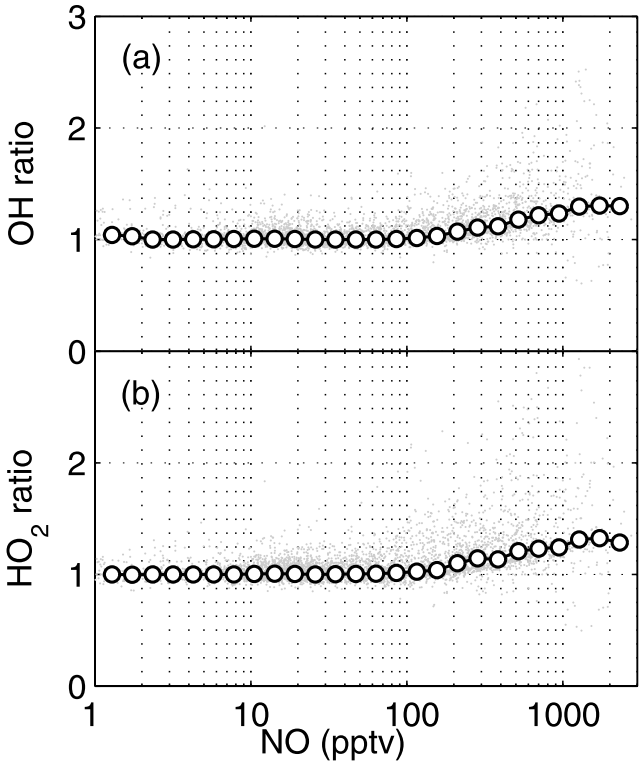

Figure 10. Ratio of constrained-to-unconstrained models for (a) OH and (b) HO_2 as a function of NO. Individual 1-min comparisons are presented (gray dots) as well as median values (circles and lines).

the planetary boundary layer. The location of these large ratios coincides with forested regions where isoprene is abundant, primarily from the Gulf Coast states up through Appalachia and the Midwest. The observed-to-modeled OH ratio is a strong function of isoprene (Figure 11). It increases slowly from 1.0 to 1.5 as isoprene increases from less than 10 pptv to 500 pptv, but for isoprene levels exceeding 500 pptv, the observed-to-modeled OH ratio rapidly increased to ~5 as isoprene increases. The observed and modeled OH levels diverge for isoprene levels greater than 100 pptv (Figure 11). This underprediction of OH is consistence with the underprediction of HO_2 below 2 km altitude. As shown in Table 1, 56% of the measured HO_2 is greater than the modeled HO_2 times 1.32.

[59] This observation from INTEX-A is consistent with tower-based observations made with a different configuration of the same instrument. In the summers of 1998 and 2000, OH and isoprene measurements were made on a tower at the PROPHET site in a Michigan forest [*Tan et al.*, 2001b]. The median daytime (SZA < 60°) observed-to-modeled OH ratio depends on isoprene in a way that is consistent with and overlaps the INTEX-A measurements (Figure 11).

[60] The reasons for the higher-than-expected OH at high isoprene levels are not clear, but most likely are due to a missing OH source in the model. For PROPHET, the agreement between observed and modeled OH is improved by introducing additional terpenes that react with O_3 to form OH [*Tan et al.*, 2001b]. In addition, the difference between the observed and calculated OH reactivity is consistent with the emissions of unmeasured terpene such as terpinolene in terms of its reaction rate with O_3 to that with OH and OH yield in the O_3 reaction [*Di Carlo et al.*, 2004]. The missing OH source can also be the OH production in the HO_2 reactions with certain RO_2, in which a significant OH yield was suggested by *Hasson et al.* [2004]. An error in our understanding of the rate coefficients or products of these kinds of reactions might cause models to predict too little OH [*Thornton et al.*, 2002], though our initial model analysis could not reconcile the missing OH source with this feedback. Another possible missing OH source over forests is the photolysis of HONO [*Zhou et al.*, 2002; *Kleffmann et al.*, 2005; *Stemmler et al.*, 2006]. While the OH was severely underpredicted in PROPHET by a model that included HONO measurements, for INTEX-A, the possible contribution of HONO to the missing OH source cannot be ruled out because no HONO measurements were made on the NASA DC-8. That the underpredicted OH was observed over several forested areas during INTEX-A provides strong evidence that this effect is not specific only to the PROPHET site in northern lower Michigan, but is, in

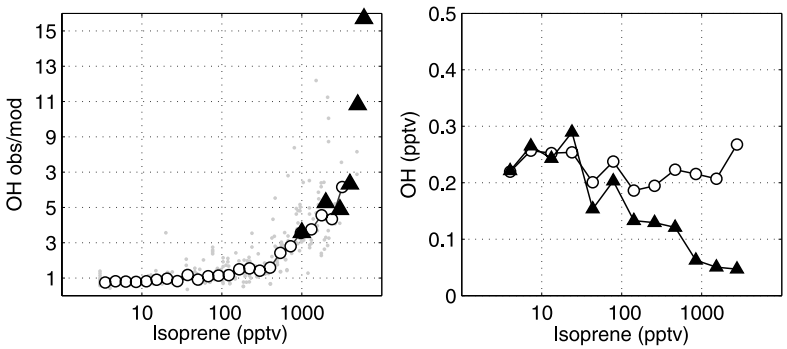

Figure 11. (left) The observed-to-modeled OH ratio as a function of isoprene. Individual 1-min measurements (gray points) and median values for isoprene intervals (circles) are shown for data taken at less than 1 km altitude and solar zenith angle less than 60°. Median observed-to-modeled OH ratios from the PROPHET tower in a Michigan forest in summer 2000 are also shown (triangles). (right) The median observed OH (circles) and modeled OH (triangles) as a function of isoprene.

fact, a more widespread property of atmospheric chemistry over forests.

5. Summary and Conclusions

[61] Measurements of OH and HO_2 were compared to the model calculations in the INTEX-A summer 2004 campaign. This study provides an excellent opportunity to test oxidation chemistry throughout the troposphere. The following conclusions can be drawn from this study.

[62] First, for most of the troposphere, observed OH and HO_2 agree well with model calculations. On average observed OH was 0.95 of modeled OH and observed HO_2 was 1.28 of modeled HO_2. This observed-to-modeled comparison is similar to that for TRACE-P, another midlatitude study for which the median observed-to-modeled ratio was 1.08 for OH and 1.34 for HO_2, and to that for PEM-TB, a tropical study for which the median observed-to-modeled ratio was 1.17 for OH and 0.97 for HO_2. In contrast, above 8 km during INTEX-A, the median observed-to-modeled HO_2 ratio increased from about 1.2 at 8 km to about 3 at 11 km.

[63] Second, an HO_x budget analysis shows that the main HO_x sources are O_3 photolysis followed by the $O(^1D) + H_2O$ reaction below 7 km and the photolysis of HCHO above 7 km. The main HO_x sinks are the HO_2-RO_2 self-reactions below 8 km and OH + NO_x reactions above 8 km.

[64] Third, an O_3 budget analysis shows that the diurnally averaged net calculated O_3 loss rate was 0.8 ppbv d^{-1} at altitudes between 1 and 5 km. Above 9 km, the diurnally averaged net calculated O_3 production rate was 4.5 ppbv d^{-1} using modeled HO_2 and 11.4 ppbv d^{-1} using observed HO_2. This difference between the net calculated O_3 production from the modeled HO_2 and the observed HO_2 is significant and a concern.

[65] Fourth, the underpredicted HO_2 at altitudes above 8 km suggests the presence of an unknown HO_x source or an error in the model's chemistry involving some of the other atmospheric constituents. The concurrent increases of the observed-to-modeled HO_2 ratio and NO with altitude suggest that an unknown HO_x source comes from the convective processes that cause the enhanced NO. Evidence from the constrained and unconstrained model runs indicates that model predictions of OH and HO_2 are particularly sensitive to the NO.

[66] Fifth, the observed-to-modeled OH ratio in the planetary boundary layer in forested regions is a strong function of isoprene. It increases slowly from 1.0 to 1.5 as isoprene increases from less than 10 pptv to 500 pptv, but for isoprene levels exceeding 500 pptv, the observed-to-modeled OH ratio rapidly increased to ~5. This isoprene dependence of observed-to-modeled OH ratio is consistent with the PROPHET measurements, indicating that this underpredicted OH, if not due to instrument artifacts, occurs in widespread forested regions.

[67] It seems more likely to us that the causes of underpredicted HO_2 above 8 km are due to unknown atmospheric constituents that are acting as HO_x sources or OH sinks or to unknown reactions and not to large errors in the measurements of either atmospheric constituents or the photochemical rate coefficients. These two major differences between observed and modeled HO_x, underpredicted HO_2 above 8 km and underpredicted OH in the planetary boundary layer in forested regions, appear to have different causes.

[68] Because the underpredicted HO_2 above 8 km and underpredicted OH above forests have strong implications for understanding global-scale tropospheric oxidation chemistry, finding the causes for these differences should be a high priority. Progress in resolving these discrepancies requires a focused research activity devoted to further examination of possible unknown OH sinks and HO_x sources.

[69] **Acknowledgments.** The work was supported by the NASA Tropospheric Chemistry Program. The authors would like to thank the DC-8 crew and support staff during the INTEX-A preparation and deployment periods for making this work possible.

References

Bertram, T. H., et al. (2007), Direct measurement of the convective recycling of the upper troposphere, *Science*, *315*, 816–820, doi:10.1126/science.1134548.

Bloss, W. J., J. D. Lee, D. E. Heard, R. A. Salmon, S. J.-B. Bauguitte, H. K. Roscoe, and A. E. Jones (2007), Observations of OH and HO_2 radicals in coastal Antarctica, *Atmos. Chem. Phys.*, *7*, 4171–4185.

Brune, W. H., et al. (1998), Airborne in-situ OH and HO_2 observations in the cloud-free troposphere and lower stratosphere during SUCCESS, *Geophys. Res. Lett.*, *25*, 1701–1704.

Brune, W. H., et al. (1999), OH and HO_2 chemistry in the North Atlantic free troposphere, *Geophys. Res. Lett.*, *26*, 3077–3080.

Carslaw, N., P. J. Jacobs, and M. J. Pilling (1999), Modeling OH, HO_2, and RO_2 radicals in the marine boundary layer: 2. Mechanism reduction and uncertainty analysis, *J. Geophys. Res.*, *104*, 30,257–30,273.

Crawford, J., et al. (1999), Assessment of upper tropospheric HO_x source over the tropical Pacific based on NASA GTE/PEM data: Net effect on HO_x and other photochemical parameters, *J. Geophys. Res.*, *104*, 16,255–16,273.

Davis, D. D., et al. (2003), An assessment of western North Pacific ozone photochemistry based on springtime observations from NASA's PEM-West B (1994) and TRACE-P (2001) field studies, *J. Geophys. Res.*, *108*(D21), 8829, doi:10.1029/2002JD003232.

Di Carlo, P., et al. (2004), Missing OH reactivity in a forest: evidence for unknown reactive biogenic VOCs, *Science*, *304*, 722–725.

Eisele, F. L., et al. (2001), Relationship between OH measurements on two different NASA aircraft during PEM Tropics B, *J. Geophys. Res.*, *106*, 32,683–32,689.

Eisele, F. L., et al. (2003), Summary of measurement intercomparisons during TRACE-P, *J. Geophys. Res.*, *108*(D20), 8791, doi:10.1029/2002JD003167.

Faloona, I. C., et al. (2004), A laser-induced fluorescence instrument for detecting tropospheric OH and HO_2: Characteristics and calibration, *J. Atmos. Chem.*, *47*, 139–167.

Folkins, I., P. O. Wennberg, T. F. Hanisco, J. G. Anderson, and R. J. Salawitch (1997), OH, HO_2, and NO in two biomass burning plumes: Sources of HO_x and implications for ozone production, *Geophys. Res. Lett.*, *24*, 3185–3188.

Hanisco, T. F., J. B. Smith, R. M. Stimpfle, D. M. Wilmouth, J. G. Anderson, E. C. Richard, and T. P. Bui (2002), In situ observations of HO_2 and OH obtained on the NASA ER-2 in the high-ClO conditions of the 1999/2000 Arctic polar vortex, *J. Geophys. Res.*, *107*(D20), 8283, doi:10.1029/2001JD001024.

Hard, T. M., R. J. O'Brien, C. Y. Chan, and A. A. Mehrabzadeh (1984), Tropospheric free radical determination by FAGE, *Environ. Sci. Technol.*, *18*, 768–777.

Hasson, A. S., G. S. Tyndall, and J. J. Orlando (2004), A product yield study of the reaction of HO_2 radicals with ethyl peroxy ($C_2H_5O_2$), acetyl peroxy ($CH_3C(O)O_2$), and acetonyl peroxy ($CH_3C(O)CH_2O_2$) radicals, *J. Phys. Chem. A*, *108*, 5979–5989.

Jacob, D. J., J. H. Crawford, M. M. Kleb, V. S. Connors, R. J. Bendura, J. L. Raper, G. W. Sachse, J. C. Gille, L. Emmons, and C. L. Heald (2003), Transport and Chemical Evolution over the Pacific (TRACE-P) aircraft mission: Design, execution, and first results, *J. Geophys. Res.*, *108*(D20), 9000, doi:10.1029/2002JD003276.

Jaeglé, L., et al. (2000), Photochemistry of HO_x in the upper troposphere at northern midlatitudes, *J. Geophys. Res.*, *105*, 3877–3892.

Jaeglé, L., D. J. Jacob, W. H. Brune, and P. O. Wennberg (2001), Chemistry of HO_x radicals in the upper troposphere, *Atmos. Environ.*, *35*, 469–489.

Kim, S., et al. (2007), Measurement of HO_2NO_2 in the free troposphere during the Intercontinental Chemical Transport Experiment–North America 2004, *J. Geophys. Res.*, *112*, D12S01, doi:10.1029/2006JD007676.

Kleffmann, J., T. Gavriloaiei, A. Hofzumahaus, F. Holland, R. Koppmann, L. Rupp, E. Schlosser, M. Siese, and A. Wahner (2005), Daytime formation of nitrous acid: A major source of OH radicals in a forest, *Geophys. Res. Lett.*, *32*, L05818, doi:10.1029/2005GL022524.

Kleinman, L. I., P. H. Daum, Y. Lee, L. J. Nunnermacker, S. R. Springston, J. Weinstein-Lloyd, and J. Rudolph (2002), Ozone production efficiency in an urban area, *J. Geophys. Res.*, *107*(D23), 4733, doi:10.1029/2002JD002529.

Madronich, S., and S. Flocke (1998), The role of solar radiation in atmospheric chemistry, in *Handbook of Environmental Chemistry*, edited by P. Boule, pp. 1–26, Springer, New York.

McKeen, S. A., et al. (1997), Photochemical modeling of hydroxyl and its relationship to other species during the Tropospheric OH Photochemistry Experiment, *J. Geophys. Res.*, *102*, 6467–6493.

Murphy, J. G., J. A. Thornton, P. J. Wooldridge, D. A. Day, R. S. Rosen, C. Cantrell, R. E. Shetter, B. Lefer, and R. C. Cohen (2004), Measurements of the sum of HO_2NO_2 and $CH_3O_2NO_2$ in the remote troposphere, *Atmos. Chem. Phys.*, *4*, 377–384.

Olson, J. R., et al. (2001), Seasonal differences in the photochemistry of the South Pacific: A comparison of observations and the model results fro PEM-Tropics A and B, *J. Geophys. Res.*, *106*, 32,749–32,766.

Olson, J. R., et al. (2004), Testing fast photochemical theory during TRACE-P based on measurements of OH, HO_2, and CH_2O, *J. Geophys. Res.*, *109*, D15S10, doi:10.1029/2003JD004278.

Olson, J. R., J. H. Crawford, G. Chen, W. H. Brune, I. C. Faloona, D. Tan, H. Harder, and M. Martinez (2006), A reevaluation of airborne HO_x observations from NASA field campaigns, *J. Geophys. Res.*, *111*, D10301, doi:10.1029/2005JD006617.

Raper, J. L., et al. (2001), Pacific Exploratory Mission in the Tropical Pacific: PEM-Tropics B, March–April 1999, *J. Geophys. Res.*, *106*, 32,401–32,425.

Ren, X., G. D. Edwards, C. A. Cantrell, R. L. Lesher, A. R. Metcalf, T. Shirley, and W. H. Brune (2003), Intercomparison of peroxy radical measurements at a rural site using laser-induced fluorescence and Peroxy Radical Chemical Ionization Mass Spectrometer (PerCIMS) techniques, *J. Geophys. Res.*, *108*(D19), 4605, doi:10.1029/2003JD003644.

Ren, X., H. Harder, M. Martinez, I. Faloona, D. Tan, R. L. Lesher, P. Di Carlo, J. B. Simpas, and W. H. Brune (2004), Interference testing for atmospheric HO_x measurements by laser-induced fluorescence, *J. Atmos. Chem.*, *47*, 169–190.

Shetter, R. E., and M. Muller (1999), Photolysis frequency measurements using actinic flux spectroradiometry during the PEM-Tropics mission: Instrumentation description and some results, *J. Geophys. Res.*, *104*, 5647–5661.

Singh, H. B., M. Kandaidou, P. J. Crutzen, and D. J. Jacob (1995), High concentrations and photochemical fate of oxygenated hydrocarbons in the global troposphere, *Nature*, *378*, 50–54.

Singh, H. B., W. H. Brune, and J. H. Crawford (2003), Reactive nitrogen and hydrogen in the global atmosphere: Progress in measurements and theory, in *Recent Advances in Atmospheric and Oceanic Sciences—Part II: Air Pollution Studies*, *Proc. Indian Natl. Sci. Acad.*, *69*(6), 669–683.

Singh, H. B., W. H. Brune, J. H. Crawford, D. J. Jacob, and P. B. Russell (2006), Overview of the Summer 2004 Intercontinental Chemical Transport Experiment-North America (INTEX-A), *J. Geophys. Res.*, *111*, D24S01, doi:10.1029/2006JD007905.

Stemmler, K., M. Ammann, C. Donders, J. Kleffmann, and C. George (2006), Photosensitized reduction of nitrogen dioxide on humic acid as a source of nitrous acid, *Nature*, *440*, 195–198, doi:10.1038/nature04603.

Tan, D., et al. (2001a), OH and HO_2 in the tropical Pacific: Results from PEM Tropics B, *J. Geophys. Res.*, *106*, 32,667–32,681.

Tan, D., et al. (2001b), HO_x budgets in a deciduous forest: Results from the PROPHET summer 1998 campaign, *J. Geophys. Res.*, *106*, 24,407–24,427.

Thompson, A. M., and R. W. Stewart (1991), Effect of chemical kinetics uncertainties on calculated constituents in a tropospheric photochemical model, *J. Geophys. Res.*, *96*, 13,089–13,108.

Thornton, J. A., P. J. Wooldridge, and R. C. Cohen (2000), Atmospheric NO_2: In situ laser-induced fluorescence detection at parts per trillion mixing ratios, *Anal. Chem.*, *72*, 528–539.

Thornton, J. A., et al. (2002), Ozone production rates as a function of NO_x abundances and HO_x production rates in the Nashville urban plume, *J. Geophys. Res.*, *107*(D12), 4146, doi:10.1029/2001JD000932.

Wennberg, P. O., et al. (1998), Hydrogen radicals, nitrogen radicals, and the production of O_3 on the upper troposphere, *Science*, *279*, 49–53.

Zhou, X., K. Civerolo, H. Dai, G. Huang, J. Schwab, and K. Demerjian (2002), Summertime nitrous acid chemistry in the atmospheric boundary layer at a rural site in New York State, *J. Geophys. Res.*, *107*(D21), 4590, doi:10.1029/2001JD001539.

M. A. Avery, J. D. Barrick, G. Chen, J. H. Crawford, J. R. Olson, G. W. Sachse, and G. S. Diskin, Science Directorate, NASA Langley Research Center, Hampton, VA 23681, USA.

D. R. Blake, Department of Chemistry, University of California, Irvine, CA 92697, USA.

W. H. Brune, Z. Chen, R. B. Long, and J. Mao, Department of Meteorology, Pennsylvania State University, University Park, PA 16802, USA.

R. C. Cohen, Department of Chemistry, University of California, Berkeley, CA 94720, USA.

A. Fried, Earth Observing Laboratory, National Center for Atmospheric Research, Boulder, CO 80307, USA.

B. Heikes, Graduate School of Oceanography, University of Rhode Island, Narragansett, RI 02881, USA.

L. G. Huey, School of Earth and Atmospheric Sciences, Georgia Institute of Technology, Atlanta, GA 30332, USA.

X. Ren, Rosenstiel School of Marine and Atmospheric Sciences, University of Miami, Miami, FL 33149, USA. (xren@rsmas.miami.edu)

H. B. Singh, NASA Ames Research Center, Moffett Field, CA 94035, USA.

R. E. Shetter, National Suborbital Education and Research Center, University of North Dakota, Grand Forks, ND 58202, USA.

P. O. Wennberg, Division of Engineering and Applied Sciences, California Institute of Technology, Pasadena, CA 91125, USA.